CHEMISTRY OF MATERIALS

Article

pubs.acs.org/cm

Thermodynamic and Electrochemical Properties of the Li–Co–O and Li–Ni–O Systems

Keke Chang,* Bengt Hallstedt, and Denis Music

Materials Chemistry, RWTH Aachen University, D-52056 Aachen, Germany

ABSTRACT: The Li–Co–O and Li–Ni–O systems, used as cathodes in lithium ion batteries, have been investigated by means of *ab initio* calculations and empirical methods. An approach based on *ab initio* calculations to obtain accurate enthalpies of formation for transition metal oxides is proposed. With the obtained enthalpies of formation and the empirical entropy data, the Gibbs energy functions of the binary and ternary oxides in the Li–Co–O and Li–Ni–O systems are determined. To prove the accuracy of this thermodynamic model, we calculate the cell voltages of lithium ion batteries. Compared to the previously calculated results, which underestimate the cell voltages of lithium ion batteries, our calculations are in good agreement with the experimental data. The present theoretical approaches are reliable to evaluate the thermodynamic and electrochemical properties of lithium-containing transition metal oxides.

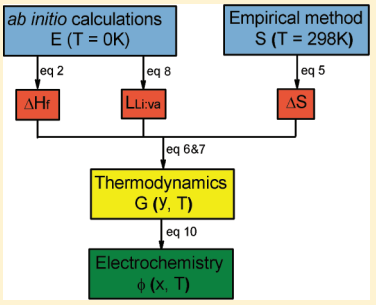

KEYWORDS: *Li–Co–O system, Li–Ni–O system, ab initio, enthalpy of formation, metal oxides, cell voltage*

INTRODUCTION

Li–M–O (M = transition metal) phases are widely applied as cathodes in lithium ion batteries. Knowledge of thermodynamic properties of Li–M–O (M = transition metal) phases is fundamental to study the stability and capacity of lithium ion batteries. The Gibbs energy functions of these phases are essential to predict the cell voltages and study the electrochemical properties of lithium ion batteries. Thus, it is our aim to establish a thermodynamic database for multicomponent Li-containing oxide systems by the calculation of phase diagrams (CALPHAD) approach.

Usually, the CALPHAD approach needs reliable experimentally thermodynamic data as input parameters to be optimized. When experimental information is scarce or completely lacking, it is necessary to estimate the thermodynamic data by *ab initio* calculations or empirical methods. It has been demonstrated that *ab initio* calculations provide a successful way of predicting the thermodynamic data, not only for metallic compounds,[1−3] but also for metal carbides.[4,5] However, extensive work by the Ceder Group shows that the pure density functional theory (DFT) method cannot directly be used to obtain accurate enthalpies of formation for metal oxides.[6,7] Also, their calculations on electrochemistry underestimate the cell voltages of lithium ion batteries.[8−12]

To better understand the thermodynamic properties of metal oxides, Wang et al.[6] introduced a certain correction for the O_2 molecule and applied the DFT+U method.[13] However, it is not a universal method because the U value for a certain transition metal is unfixed.[6,14−18] For instance, when performing *ab initio* calculations on the thermodynamic property, phase diagram and electrochemical property of the Li–Co–O system, three different U values are determined for Co in their work.[6,14,16] Thus, if an inappropriate U value is set, inaccurate results will limit us to study the properties of cathodes in lithium ion batteries.

The purpose of the present work is to (1) provide an appropriate approach to accurately calculate the enthalpies of formation for transition metal-containing oxides and (2) determine the Gibbs energy functions of the binary and ternary oxides in the Li–Co–O and Li–Ni–O systems. These are then used for calculations of cell voltages to study the electrochemical properties of lithium ion batteries.

METHODS

Enthalpies of Formation: *Ab Initio* Calculations. *Ab initio* calculations were carried out using DFT, as implemented in the Vienna *ab initio* simulation package (VASP).[19] The valence electrons were explicitly treated by projector augmented plane-wave (PAW) potentials.[20] The generalized gradient approximation (GGA) method was performed with the Blöchl corrections for the total energy.[21] A plane-wave cutoff energy of 500 eV and an energy convergence criterion of 0.01 meV for electronic structure self-consistency were used in the calculations. The integration in the Brillouin zone was done on appropriate *k*-points, which was determined after Monkhorst–Pack.[22] Because magnetic contributions to the total energy are significant, spin polarization effects were included.

Because solely the GGA+U approach did not give rise to accurate enthalpies of formation for metal oxides,[6] we probed a series of oxides without the Hubbard correction in order to unravel this issue. The enthalpies of formation at 0 K were calculated for binary oxides of 14 metal elements (Li, Na, Mg, Al, K, Ca, V, Cr, Mn, Fe, Co, Ni, Cu, and Zn). Because Ti exhibits weakly localized 3*d* electrons, which is different from other transition metals,[7] Ti oxides were not studied in this work. Sc_2O_3 possesses a different structure from other transition metal oxides and thus was not considered. The studied oxides were

Received: July 10, 2011
Revised: November 29, 2011
Published: November 30, 2011

Table 1. Structural Data for Lithium Cobalt Oxides and Lithium Nickel Oxides[a]

phase	structure	space group	lattice parameters (Å)			ref
			a	*b*	*c*	
Li_2O	fluorite	$Fm\bar{3}m$	4.610	4.660	4.610	ref 23
			4.660	4.610	4.660	this work
Li_2O_2	hexagonal	$P6_3/mmc$	3.153	3.153	7.771	ref 24
			3.186	3.186	7.742	this work
CoO	rocksalt	$Fm\bar{3}m$	4.240	4.240	4.240	ref 25
			4.222	4.222	4.222	this work
NiO	rocksalt	$Fm\bar{3}m$	4.152	4.152	4.152	ref 26
			4.164	4.164	4.164	this work
Co_2O_3	corundum	$R\bar{3}c$	4.875	4.875	12.960	ref 27
			4.875	4.875	12.712	this work
Co_3O_4	spinel	$Fd\bar{3}m$	8.065	8.065	8.065	ref 28
			8.101	8.101	8.101	this work
O1-CoO_2	layered O1	$P\bar{3}m1$	2.820	2.820	4.238	ref 29
			2.824	2.824	4.405	this work
O1-NiO_2	layered O1	$P\bar{3}m1$	2.818	2.818	4.367	ref 30
			2.822	2.822	4.563	this work
O2-CoO_2	layered O2	$P6_3mc$	2.808	2.808	8.489	this work
O3-CoO_2	layered O3	$R\bar{3}m$	2.822	2.822	12.879	ref 31
			2.822	2.822	13.150	this work
O3-NiO_2	layered O3	$R\bar{3}m$	2.835	2.835	14.332	ref 32
			2.831	2.831	13.804	this work
O2-$LiCoO_2$	layered O2	$P6_3mc$	2.802	2.802	9.536	ref 33
			2.817	2.817	9.538	this work
O3-$LiCoO_2$	layered O3	$R\bar{3}m$	2.814	2.814	14.050	ref 29
			2.831	2.831	14.255	this work
O3-$LiNiO_2$	layered O3	$R\bar{3}m$	2.877	2.877	14.188	ref 34
			2.897	2.897	14.348	this work
s-$LiCoO_2$	spinel	$Fd\bar{3}m$	8.009	8.009	8.009	ref 35
			8.130	8.130	8.130	this work
s-$LiNiO_2$	spinel	$Fd\bar{3}m$	8.207	8.207	8.207	ref 36
			8.183	8.183	8.183	this work
$LiCo_2O_4$	spinel	$Fd\bar{3}m$	8.002	8.002	8.002	ref 37
			8.025	8.025	8.025	this work
$LiNi_2O_4$	spinel	$Fd\bar{3}m$	8.190	8.190	8.190	ref 38
			8.111	8.111	8.111	this work
m-Li_4CoO_4[b]	monoclinic	$P2_1/m$	5.340	6.160	5.180	ref 39
			5.425	6.258	5.263	this work
t-Li_6CoO_4	tetragonal	$P4_2/nmc$	6.544	6.544	4.651	ref 40
			6.694	6.694	4.607	this work

[a]Lattice parameters from literature are experimental results. [b]For this phase, the experimental β is 90.4°, while the calculated value is 90.3°.

separated into two groups. The first one comprised oxides of nontransition metals (Li, Na, Mg, Al, K, Ca, Cu, and Zn), while the other one included oxides of transition metals (Cr, Mn, Fe, Co, and Ni). Although Cu and Zn are transition metals, they have completely filled 3*d* shells and have different properties (the maximum valence state is +2) compared to other transition metals, their oxides were considered as nontransition metal oxides in this work. The crystal structures and magnetic configurations of the binary metal oxides are accepted from ref 6. Table 1 summarizes the structural data for lithium cobalt oxides and lithium nickel oxides. For the lattice parameters, the difference between the calculated and experimental values was within the range −0.96~4.48%.

The enthalpy of formation (per metal) for the binary oxide, MO_n, was calculated using the following expression:

$$\Delta H_f(MO_n) = E(MO_n) - [E(M) + 0.5nE(O_2)] \quad (1)$$

where $E(MO_n)$, $E(M)$, and $E(O_2)$ denote the total energies of MO_n, M, and O_2, respectively. To calculate $E(O_2)$, 10 × 10 × 10 Å^3 supercells were used to diminish the long-range interactions due to periodic boundary conditions imposed within the VASP code. The total energy of a single oxygen atom was also calculated, and then, the binding energy of the O_2 molecule was obtained. Similarly, the enthalpy of formation for the Li-transition metal oxide, $Li_xM_yO_z$ (M = Co, Ni), was calculated as follows:

$$\Delta H_f(Li_xM_yO_z) = E(Li_xM_yO_z) - [x_{Li}E(Li) + x_ME(M) + 0.5x_OE(O_2)] \quad (2)$$

where $E(Li_xM_yO_z)$, $E(Li)$, $E(M)$, and $E(O_2)$ denote the total energies of MO_n, Li, M, and O_2, respectively.

Entropies of Formation: Empirical Predictions. Considering the absence of experimental data and reliable calculations, it is necessary to estimate the entropies of metal oxides at 298 K by empirical methods. There are several publications concerning the estimation of standard entropy data of inorganic compounds,[41−44] showing reasonable agreements between the estimated and known

dx.doi.org/10.1021/cm201964r | Chem. Mater. 2012, 24, 97−105

experimental results. Thus, the method suggested by Kubaschewski et al.[44] was applied in the present work. The entropy data of the oxide, MO_n, can be derived from the values of the anionic and cationic contributions using the following expression:

$$S(MO_n) = S(M) + nS(O) \quad (3)$$

where $S(M)$ and $S(O)$ denote the anionic and cationic contributions, respectively, which can directly be read from the tables in ref 44. Similarly, the entropy data can be obtained for the Li-transition metal oxide, $Li_xM_yO_z$ (M = Co, Ni). Then, the entropies of formation for the oxides can be expressed as follows:

$$\Delta S(MO_n) = S(MO_n) - [S(M) + 0.5nS(O_2)] \quad (4)$$

$$\Delta S(Li_xM_yO_z) = S(Li_xM_yO_z) - [x_{Li}S(Li) + x_{Co}S(M) + 0.5x_OS(O_2)] \quad (5)$$

where $S(Li)$, $S(M)$, and $S(O_2)$ denote the standard entropies of Li, M, and O_2 in the reference states, respectively.

Gibbs Energy Functions and Cell Voltage Calculation. For stoichiometric $Li_xM_yO_z$ (M = Co, Ni) phases, the Neumann–Kopp rule was applied for the heat capacity,[44] so the Gibbs energy function can be expressed as follows (taking $Li_xCo_yO_z$ as an example):

$$^\circ G_m^{Li_xCo_yO_z} - x_{Li}\,^\circ G_{Li}^{BCC\,A2} - x_{Co}\,^\circ G_{Co}^{HCP\,A3} - 0.5x_O\,^\circ G_{O_2}^{GAS} = \Delta H - \Delta ST \quad (6)$$

where ΔH, ΔS, and T denote the enthalpy of formation, the entropy of formation, and the temperature, respectively.

In lithium ion batteries, when the Li ions are deintercalated from the cathodes, vacancies form on the Li sublattice. So, the stoichiometric $Li_xM_yO_z$ phase should, in turn, be referred to the $(Li, Va)_xM_yO_z$ phase. The Gibbs energy function of $(Li, Va)_xM_yO_z$ can be determined by the following equation:

$$^\circ G_m^{(Li,Va)_xM_yO_z} = y_{Li}\,^\circ G_m^{Li_xM_yO_z} + (1 - y_{Li})\,^\circ G_m^{M_yO_z} + xRT[y_{Li}\ln y_{Li} + (1 - y_{Li})\ln(1 - y_{Li})] + y_{Li}(1 - y_{Li})L_{Li,Va:M:O} \quad (7)$$

where y_i (i = Li, Va) is the fraction of the species i in the first sublattice and $L_{Li,Va:M:O}$ is the interaction parameter between the $Li_xM_yO_z$ and M_yO_z compositions. Taking Li_xCoO_2 ($0 \le x \le 1$) as an example, $L_{Li,Va:M:O}$ can be determined by *ab initio* calculations based on regular solution approximation using the following expression:

$$x(1 - x)L_{Li,Va:M:O} = E(Li_xCoO_2) - xE(LiCoO_2) - (1 - x)E(CoO_2) \quad (8)$$

The cell voltage (φ) of an electrochemical cell can be calculated using the following equation:

$$\varphi = -\frac{\mu_{Li}^{Cathode} - \mu_{Li}^{Anode}}{zF} \quad (9)$$

where μ_{Li} is the Li chemical potential, z is the moles of electrons involved (for Li^+, $z = 1$), and F is Faraday's constant. In the present work, the calculated cell voltage (vs Li/Li^+) of a lithium ion battery can be expressed as follows:

$$\varphi = -\frac{\mu_{Li}^{Cathode}}{F} \quad (10)$$

To facilitate reading, the present theoretical approaches are summarized and shown as the flowchart shown in Figure 1.

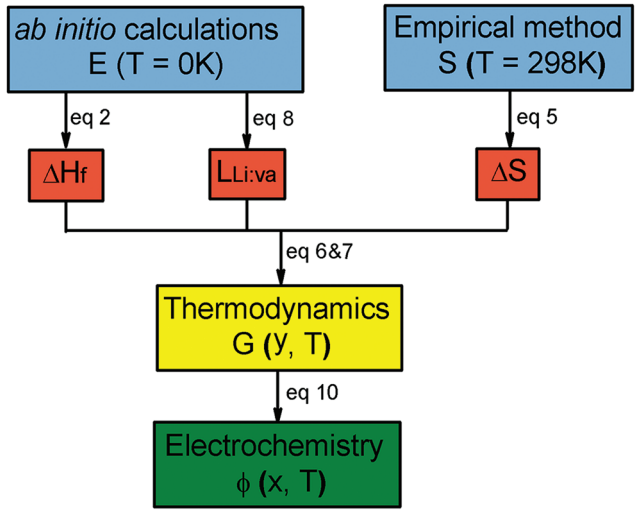

Figure 1. Flowchart of the present theoretical approaches.

RESULTS AND DISCUSSION

Enthalpies of Formation for Binary Metal Oxides. The calculated enthalpies of formation for cobalt oxides using the GGA method are shown in Figure 2. As a comparison, the

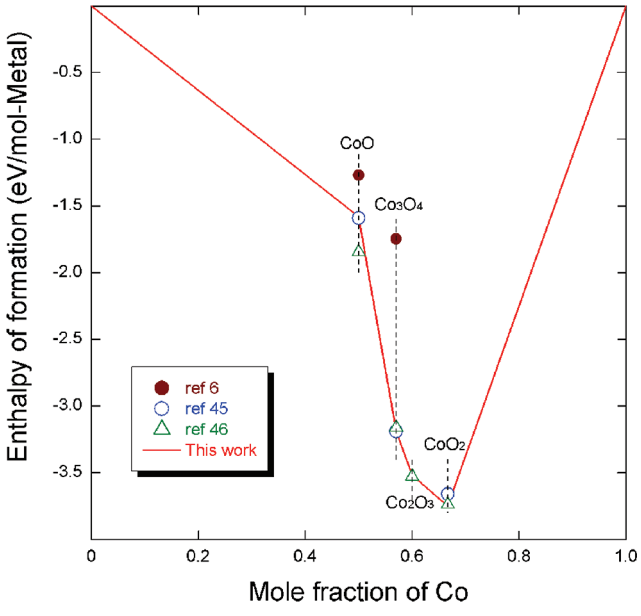

Figure 2. Calculated enthalpies of formation for cobalt oxides using the GGA method compared to the previous results.[6,45,46]

results obtained with the same method are presented.[6,45,46] It is clear that the present work is consistent with refs 45 and 46 but is not consistent with ref 6. The reason is that the binding energy of O_2 in this work is calculated to be −5.64 eV, while the result from ref 6 is −6.02 eV. Compared to experimental value (−5.23 eV), the GGA method underestimates the binding energy of O_2, which is a well-known issue for the GGA exchange–correlation treatment.[47,48] This difference leads to a deviation in the enthalpies of formation between our work and ref 6. By using a −1.36 eV energy correction for O_2 molecule, they obtain the best fit of enthalpies of formation for the non-transition metal oxides. However, the present *ab initio* results directly show reasonable

dx.doi.org/10.1021/cm201964r | *Chem. Mater.* 2012, 24, 97–105

agreement with the experimental results;[44,49] see Figure 3a. Note that refs 44 and 49 are assessments of experimental results and thus considered to be experimental data in this work.

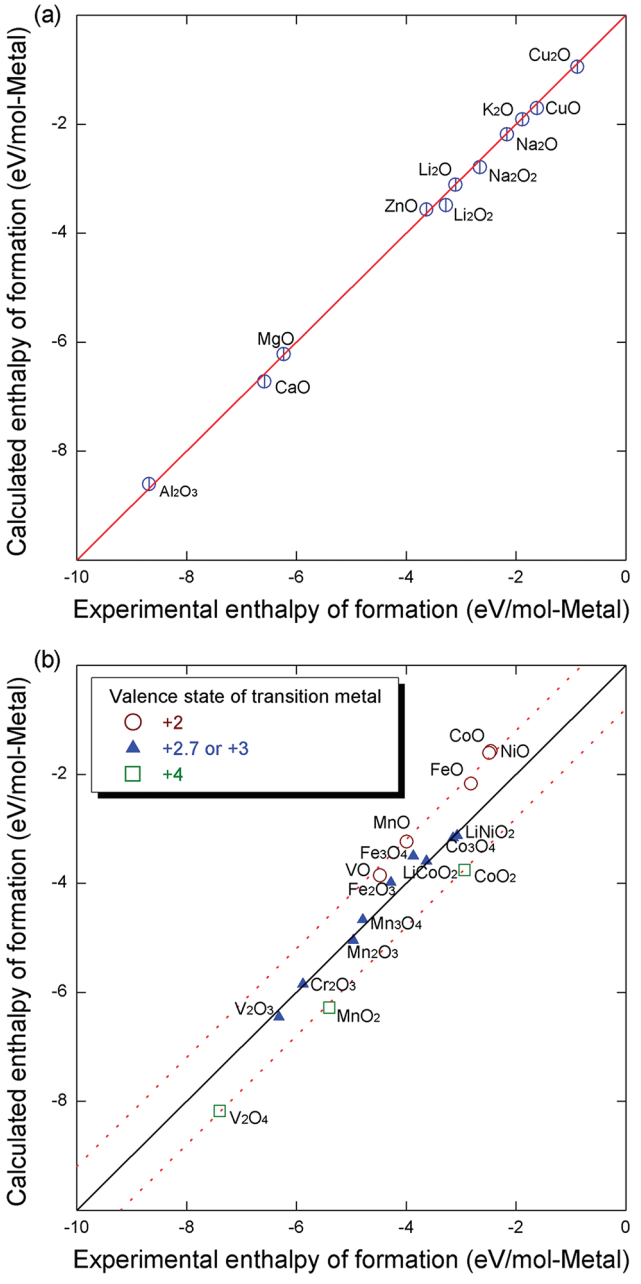

Figure 3. Calculated enthalpies of formation for (a) nontransition metal oxides compared to the experimental results and[44,49] (b) transition metal oxides compared to the experimental results.[44,49−52]

Figure 3b shows the calculated enthalpies of formation for the transition metal oxides. For the oxides of transition metals with valence state +2.7 or +3, the calculated results agree well with experimental data.[44,49−52] The exceptions are the results for iron oxides, which we will not discuss further because they are not within the scope of this work. For oxides of transition metals with valence state of +2 (MO), the calculation overestimates the enthalpies of formation, while for those with a valence state of +4 (MO_2), the calculation underestimates the enthalpies of formation. This is due to inaccuracies of the GGA method in the correlation energy of the 3*d* states in the transition metal oxides.[6,7] Strong as well as weak correlations are still a challenge for DFT. Although Wang et al.[6] suggested the GGA+U method to calculate the enthalpies of formation for transition metal oxides, it is not applied in this work. The determination of U is not straightforward,[6,14,53] and hence, we suggest the following approach. Simply and clearly from Figure 3b, we can obtain the accurately calculated enthalpy of formation per mole metal by corrections of −0.8 eV for MO and +0.8 eV for MO_2. This approach will allow us to obtain accurate results for lithium cobalt oxides and lithium nickel oxides whose experimental enthalpies of formation are lacking.

To rationalize our correction proposal, we consider an example of transition metal oxides, namely, vanadium oxides, and study their partial density of states (DOS) as given in Figure 4. Figure 4a

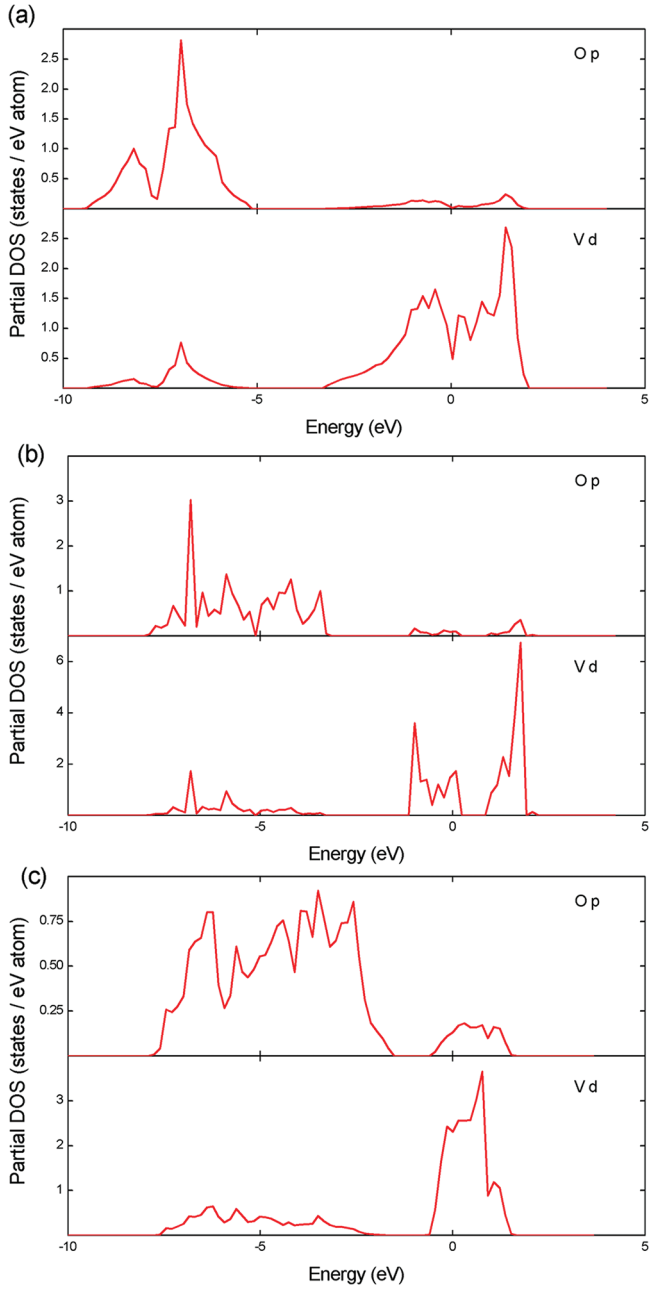

Figure 4. Partial density of states (DOS) for vanadium oxides: (a)VO; (b)V_2O_3; and (c)V_2O_4. Fermi level is set to 0 eV. Note that, for VO and V_2O_3, the partial density of V *d* states are plotted by adding the up and down spin states.

dx.doi.org/10.1021/cm201964r | *Chem. Mater.* 2012, 24, 97−105

Table 2. Summary of Thermodynamic Properties of Lithium Cobalt Oxides and Lithium Nickel Oxides

phase	enthalpy of formation (kJ/mol)	entropy of formation (J/mol·K)	method	ref
Li_2O	−598.73	−122.86	assessment[a]	ref 49
	−597	−124.25	CALPHAD	ref 57
	−599.81	−127.05	*ab initio*/EM[b]	this work
Li_2O_2	−632.62	−206.82	assessment	ref 49
	−644.28	−202.47	CALPHAD	ref 57
	−673.54	−202	*ab initio*/EM	this work
CoO	−237.7	−79.56	assessment	ref 49
	−236.86	−78.24	CALPHAD	ref 58
	−229.36	−93.95	*ab initio*/EM	this work
NiO	−239.7	−94.45	assessment[a]	ref 44
	−240.28	−95.76	CALPHAD	ref 59
	−232.05	−92.85	*ab initio*/EM	this work
Co_3O_4	−910	−385.91	assessment	ref 49
	−915.39	−390.8	CALPHAD	ref 58
	−922.84	−385.1	*ab initio*/EM	this work
O1-CoO_2	−290	−240	CALPHAD	ref 60
	−285.44	−195.2	*ab initio*/EM	this work
O1-NiO_2	−236.87	−194.1	*ab initio*/EM	this work
O2-CoO_2	−282.73	−195.2	*ab initio*/EM	this work
O3-CoO_2	−285.9	−240	CALPHAD	ref 60
	−281.92	−195.2	*ab initio*/EM	this work
O3-NiO_2	−236.08	−194.1	*ab initio*/EM	this work
O2-$LiCoO_2$	−684.41	−209.7	*ab initio*/EM	this work
O3-$LiCoO_2$	−679.4	−211.75	calorimetry	ref 52, 61
	−678	−210	CALPHAD	ref 60
	−693.41	−209.7	*ab initio*/EM	this work
O3-$LiNiO_2$	−593	–	calorimetry	ref 50
	−602.03	−208.6	*ab initio*/EM	this work
s-LiCoO2	−694.14	−209.7	*ab initio*/EM	this work
s-LiNiO2	−599.13	−208.6	*ab initio*/EM	this work
$LiCo_2O_4$	−1126.96	−403.7	*ab initio*/EM	this work
$LiNi_2O_4$	−981.87	−401.5	*ab initio*/EM	this work
m-Li_4CoO_4	−1454.16	−451.3	*ab initio*/EM	this work
m-Li_6CoO_4[c]	−1880.95	−614.8	*ab initio*/EM	this work
t-Li_4CoO_4	−1396.72	−451.3	*ab initio*/EM	this work
t-Li_6CoO_4	−1938.39	−614.8	*ab initio*/EM	this work

[a]Refs 44 and 49 are assessments of experimental results and thus considered as experimental data. [b]EM means the empirical method[44] applied in the present work. [c]This phase is a fictitious phase with the same structure as *m*-Li_4CoO_4. The enthalpy difference between *t*-Li_6CoO_4 and *m*-Li_6CoO_4 is set equal to the difference between *m*-Li_4CoO_4 and *t*-Li_4CoO_4.

shows the partial DOS for the rock-salt structured VO. It is evident that V 3*d* states are localized, but at the same time, they hybridize with O 2*p* states. For instance, this is transparent in the range from approximately −10 to −5 eV. V_2O_3 (Figure 4b) and V_2O_4 (Figure 4c) are characterized with the comparable electronic structure. As the valence of V is increased from +2 to +4, it is apparent that the hybridized V 3*d*−O 2*p* states shift toward higher energies. This, in turn, changes the nature of localized V 3*d* states. It seems that the localization of V 3*d* states in V_2O_3 gives rise to correct total energies, and hence, the enthalpy of formation agrees well with the experimental value. Obviously, one would need to shift the V 3*d* states in VO and V_2O_4, for instance using the Hubbard approach (GGA+U) or the perturbation theory. It is worth noting that shifts of different sign and magnitude may be required. The Hubbard parameter is often debated as a result of the choice of observables probed or difficult to unambiguously determine from self-consistent approaches,[53] while the perturbation theory, such as the GW approximation,[54] requires an extensive CPU time. Because these corrections are computationally demanding, we apply a very simple correction, as described above. Furthermore, our correction proposal may also explain why VO has a tendency to appear metastable in DFT calculations.[55,56] Vacancy stabilization was normally assumed for VO, but it may also be related to the inaccurate enthalpy of formation at 0 K, which can easily be corrected by our proposal.

Gibbs Energy Functions of Stoichoimetric $Li_xM_yO_z$ phases. Table 2 summarizes the calculated enthalpies of formation and entropies of formation for lithium cobalt oxides and lithium nickel oxides. Using eq 6, the Gibbs energy functions of these stoichoimetric phases can be obtained.

In practice, O3-$LiMO_2$ and *s*-$LiMO_2$ (M = Co, Ni) are referred as HT-$LiMO_2$ and LT-$LiMO_2$ which are prepared at high temperature (∼850 °C) and low temperature (∼400 °C or ∼180 °C), respectively.[35,36] According to our calculations, it is difficult to judge which phase is more stable, because the enthalpy difference between the O3-$LiMO_2$ and *s*-$LiMO_2$ phases is too small (−0.73 kJ/mol for Co and +2.9 kJ/mol for Ni containing oxides). Also, the experimental results show that the X-ray diffraction profiles of O3-$LiCoO_2$ and *s*-$LiCoO_2$ are almost identical.[62] The calculated enthalpies of formation for different structures of the MO_2 phases show that O1 is the most stable structure. This is consistent with the experimental results that O1-MO_2 forms after all Li ions are deintercalated from O3-$LiMO_2$ in the Li/O3-$LiMO_2$ battery.[30,63−66] The *t*-Li_4CoO_4 phase is isostructural with *t*-Li_6CoO_4, which forms after the Li ions are deintercalated from *t*-Li_6CoO_4 and the phase composition changes into Li_4CoO_4. The enthalpies of formation for *t*-Li_6CoO_4, *t*-Li_4CoO_4, and *m*-Li_4CoO_4 phases are also calculated for comparison. The *m*-Li_6CoO_4 phase is a fictitious phase with the same structure of *m*-Li_4CoO_4. The enthalpy difference between *t*-Li_6CoO_4 and *m*-Li_6CoO_4 is set equal to the difference between *m*-Li_4CoO_4 and *t*-Li_4CoO_4.

From Table 2, we can also see that the entropies of formation for different phases with the same components and compositions are identical. This means that for a phase, if a certain structure is stable at 0 K, compared to other structures, it will be stable at any temperature. To explain this, we take the example of Mn_3O_4, which undergoes a polymorphic transition from tetragonal α-Mn_3O_4 to cubic β-Mn_3O_4 with increasing temperature. According to eq 6, the difference between the Gibbs energy functions of tetragonal α-Mn_3O_4 and β-Mn_3O_4 is only the value of ΔH. Thus, the empirical method suggested by Kubaschewski et al.[44] cannot be used to describe the high temperature−low temperature phase transformation.

Experimental and CALPHAD results are also presented for comparison in Table 2. The presently obtained results are consistent with the experimental[44,49,50,52,61] and

dx.doi.org/10.1021/cm201964r | *Chem. Mater.* 2012, 24, 97−105

CALPHAD[57−60] results in most cases. However, there is a large disparity with the entropy of formation for the CoO_2 phase (O1-CoO_2 or O3-CoO_2). The problem is that the standard entropy data of the CoO_2 phase obtained by Abe and Koyama[60] is −4.9 J/mol·K, which is less than 0. In comparison, our result is more reasonable with the value of 39.9 J/mol·K.

Application: Predictions of Cell Voltages of Lithium Ion Batteries. To prove the accuracy of our thermodynamic model and study the electrochemical properties of the Li−Co−O and Li−Ni−O systems, we calculate the cell voltages of lithium ion batteries using the Gibbs energy function derived from eqs 7 and 8. Six lithium ion batteries are studied in the present work: Li/O3-Li_xMO_2 (M = Co, Ni; $0 \le x \le 1$), Li/$Li_xM_2O_4$ (M = Co, Ni; $1 \le x \le 2$), Li/O2-Li_xCoO_2 ($0 \le x \le 1$), and Li/$Li_{4+x}CoO_4$ ($0 \le x \le 2$). To facilitate reading, we classify them into three groups of cells, in which the cathodes have layered, spinel, and tetragonal structures, respectively.

1. Cells with a Layered Structural Cathode. Layered structural phases, especially O3-$LiCoO_2$, have been widely applied as cathodes, from which, the Li ions can easily be deintercalated. Here, we study the Li/O3-Li_xCoO_2 ($0 \le x \le 1$) cell in detail. Note that our models cannot describe the Li/vacancy ordering in the cathode; this limitation only allow us to reproduce the approximate average voltage profiles.

O3-$LiCoO_2$ is isostructural with α-$NaFeO_2$, having close-packed oxygen layers stacked in an *ABC* sequence with Li^+ and Co^{3+} residing in octahedral sites within the fcc oxide array.[8,10] During the cycling of the Li/O3-Li_xCoO_2 ($0 \le x \le 1$) cell, the reaction can be expressed as

$$LiCoO_2 \underset{\text{Discharge}}{\overset{\text{Charge}}{\rightleftharpoons}} Li_xCoO_2 + Li^+ + e$$

The structure changes during charging and discharging are presented in Figure 5a. All the phases (O1, H1−3, the monoclinic phase, and O3) except the ordered O3 phase are considered in our work. We calculate the voltage profile of this cell, shown as the solid line in Figure 5b. Although the Li/vacancy ordering is not considered, the calculated voltage profile can reflect the phase changes in the cathode during the cyclinlg of the cell. When the cell is fully charged, the cathode has O1 structure. As x in Li_xCoO_2 increases, it first changes into H1−3 phase, which has a hybrid structure of O1 and O3, as shown in Figure 5a. This phase exists at x = 0.13−0.21, according to our calculation, and at x = 0.11−0.21, according to experiments.[31] Then, the cathode changes into O3 structure. When x is about 0.5, the hexagonal O3 structure will be distorted into the monoclinic structure.[31,65,66] The experiments show that this phase exists at x = 0.43−0.52,[31] 0.47−0.52,[65] and 0.5−0.7.[66] In our calculations, we consider the monoclinic phase as a stoichoimetric $Li_{0.5}CoO_2$ phase, and it exists at x = 0.47−0.53. We also calculate the voltage profile, including only end-member phases, shown as the dashed line in Figure 5b. The profile is smooth as the phase transformations and Li/vacancy ordering are not considered. If we only compare the voltage intervals of these two lines in Figure 5b, there is little difference.

The calculated cell voltages of Li/O3-Li_xCoO_2 ($0 \le x \le 1$) and Li/O3-Li_xNiO_2 ($0 \le x \le 1$) at 300 K compared to the experimental data,[66,69−71] CALPHAD calculation,[60] and the previous theoretical results[8−10] are shown in Figure 6. The

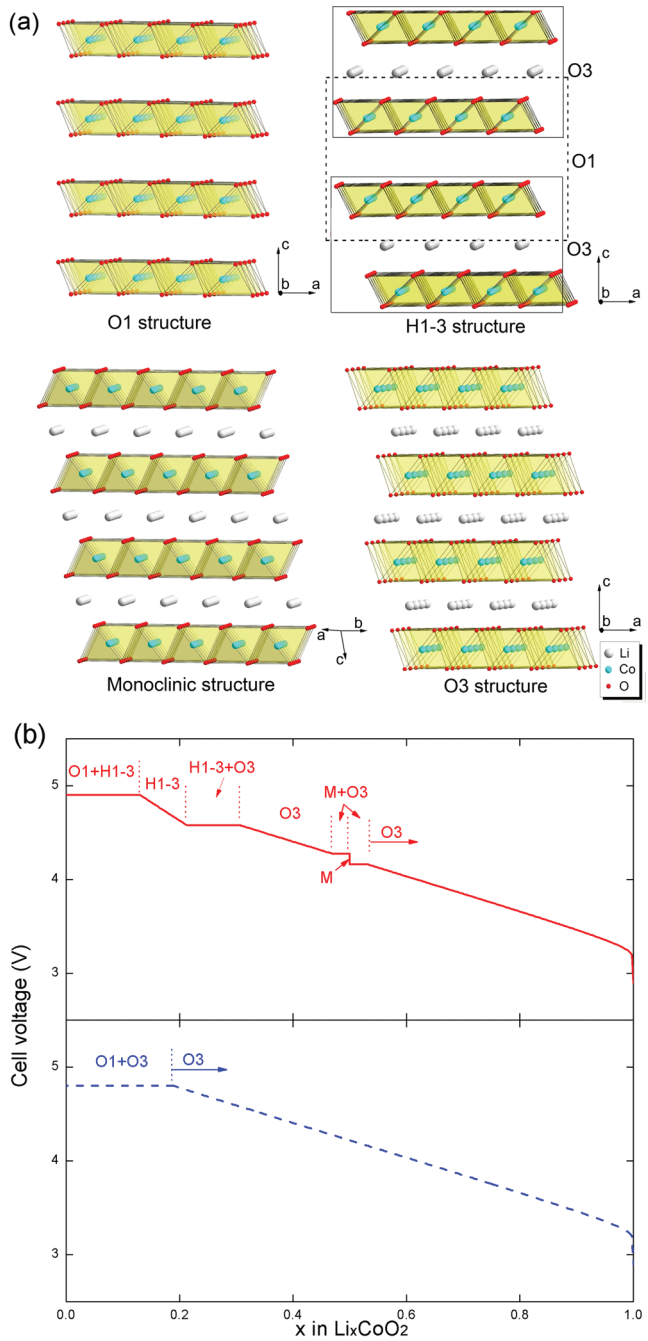

Figure 5. (a) Structure changes in the cathode: O1, H1−3, the monoclinic phase, and O3. (b) Calculated cell voltages of Li/O3−Li_xCoO_2 ($0 \le x \le 1$) at 300 K: the solid line shows the calculation including all intermediate phases without considering Li/vacancy ordering, and the dashed line shows the calculation including only end-member phases.

previous theoretical results clearly show underestimation of the cell voltages.[8−10] In comparison, the present calculations are in better agreement with the experimental[66,69−71] and CALPHAD[60] results.

Apart from O3, $LiCoO_2$ can exhibit another type of layered structure: O2. O2-$LiCoO_2$ can be prepared by Na^+/Li^+ exchange from P2−$Na_{0.7}CoO_2$.[74] Compared to O3-$LiCoO_2$, it is thermodynamically metastable. From Table 2, we can see that the calculated enthalpy difference between O2-$LiCoO_2$ and

dx.doi.org/10.1021/cm201964r | *Chem. Mater.* 2012, 24, 97−105

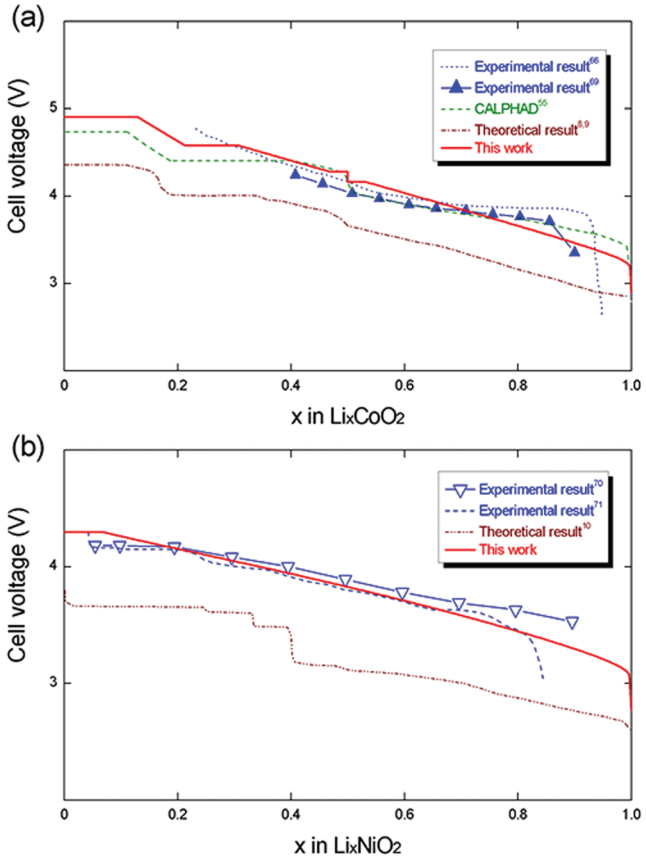

Figure 6. Calculated cell voltages of Li/O3-Li$_x$MO$_2$ (M = Co, Ni; $0 \leq x \leq 1$) at 300 K compared to the experimental data,[66,69−71] CALPHAD calculation,[60] and the previous theoretical results:[8−10] (a) Li/O3-Li$_x$CoO$_2$; (b) Li/O3-Li$_x$NiO$_2$.

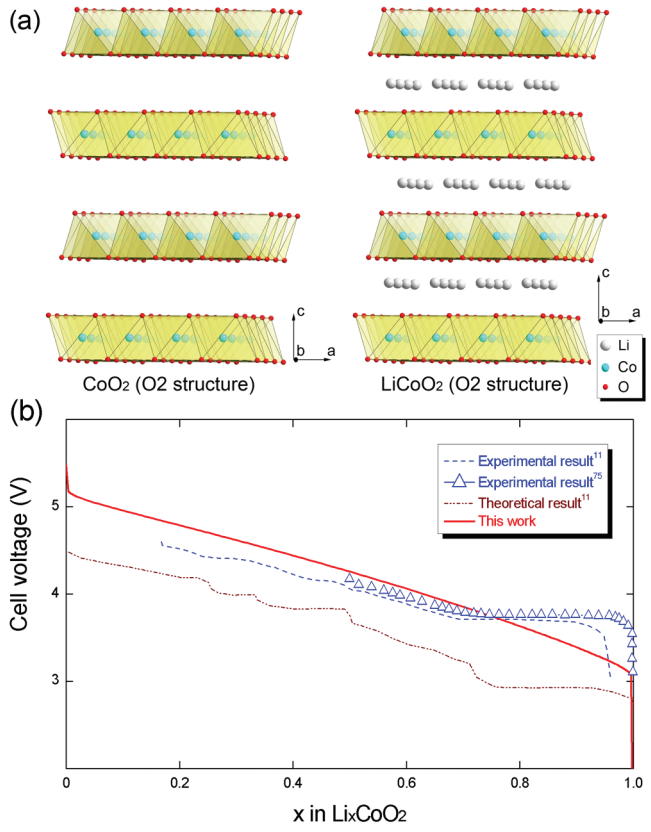

Figure 7. (a) O2 structure of Li$_x$CoO$_2$ (x = 0, 1). (b) Calculated cell voltage of the Li/O2-Li$_x$CoO$_2$ ($0 \leq x \leq 1$) battery at 300 K, as compared to the experimental data[11,75] and the previous theoretical results.[11]

O3-LiCoO$_2$ is +9.0 kJ/mol. This value is consistent with the experimentally determined value (+8.23 kJ/mol).[50] The total energy of O2-Li$_x$CoO$_2$ at x = 0.5 is obtained by *ab initio* calculations. Then, the interaction parameters $L_{Li,Va:Co:O}$ for O2-(Li,Va)CoO$_2$ is determined to be −88367 J/mol, which is similar to the previous *ab initio* result.[11] Both of the end-member phases in the cathode possess O2 structure, as shown in Figure 7a. Although the O2 structure is thermodynamically metastable, as compared with the O3 structure, there is no O2 → O3 transformation at room temperature because it requires rearrangement of the strong Co−O bonds.[11] More detailed phase transformations and Li/vacancy ordering during the cycling of the Li/O2-Li$_x$CoO$_2$ cell are discussed in ref 11. In this work, the approximate average cell voltage of Li/O2-Li$_x$CoO$_2$ ($0 \leq x \leq 1$) at 300 K is calculated and shown in Figure 7b. Compared with the previous calculation, which underestimates the cell voltage,[11] the present result shows more reasonable agreement with the experimental data.[11,75]

2. Cells with a Spinel Structural Cathode: Li/Li$_x$M$_2$O$_4$ (M = Co, Ni; 1≤x ≤ 2). Figure 8a shows the structure of the Li$_x$Co$_2$O$_4$ phase and the diffusion path of Li in the cathode. The crystal has an fcc oxygen sublattice with Co^{3+} residing in octahedral sites.[9,72] The Li ions can occupy two different sites: 8*a* tetrahedral sites and 16*c* octahedral sites.[9,72] When the Li/Li$_x$Co$_2$O$_4$ cell is fully charged, the Li ions occupy 16*c* sites. When the cell is discharged, they will diffuse into 8*a* sites and the spinel LiCo$_2$O$_4$ phase forms.[72,73] The reaction can be expressed as

$$[Li^+]_{16c}[Co_2^{3+}]_{16d}[O_4^{2-}]_{32e} \underset{\text{Discharge}}{\overset{\text{Charge}}{\rightleftharpoons}} [Li^+]_{8a}[Co^{3+}Co^{4+}]_{16d}[O_4^{2-}]_{32e} + Li^+ + e$$

Although experimental results show that the Li ions can be deintercalated from the LiCo$_2$O$_4$ phase,[62,73] we only calculate the cell voltages of Li/Li$_x$Co$_2$O$_4$ at $1 \leq x \leq 2$. One reason is that the reported cell voltage curves are quite different.[62,73] Another reason is that the end-member phase, which forms after all the Li ions are deintercalated, is not experimentally determined. The total energy of Li$_{1.5}$Co$_2$O$_4$ is calculated and then the interaction parameter $L_{Li,Va:Co:O}$ for LiCo$_2$O$_4$ and *s*-LiCoO$_2$ is determined to be −28 495 J/mol. The calculated cell voltage of Li/Li$_x$Co$_2$O$_4$ at 300 K is shown in Figure 8b, which reproduces the most recent experimental result quite well.[72] A similar calculation is performed for Li/Li$_x$Ni$_2$O$_4$ (the calculated $L_{Li,Va:Ni:O}$ is −3313 J/mol), also consistent with the experimental result,[36] see Figure 8b.

3. Cell with a Tetragonal Structural Cathode: Li/Li$_{4+x}$CoO$_4$ (0 ≤ x ≤ 2). The research work shows that *t*-Li$_6$CoO$_4$ is a good candidate for cathodes in lithium ion batteries.[76] The antifluorite structure, as shown in Figure 9a, facilitates Li^+ deintercalation and subsequent Li^+ intercalation in the phase.[76] When the cell is charged, a distortion occurs and the tetragonal phase transforms into the monoclinic phase,

dx.doi.org/10.1021/cm201964r | *Chem. Mater.* 2012, 24, 97−105

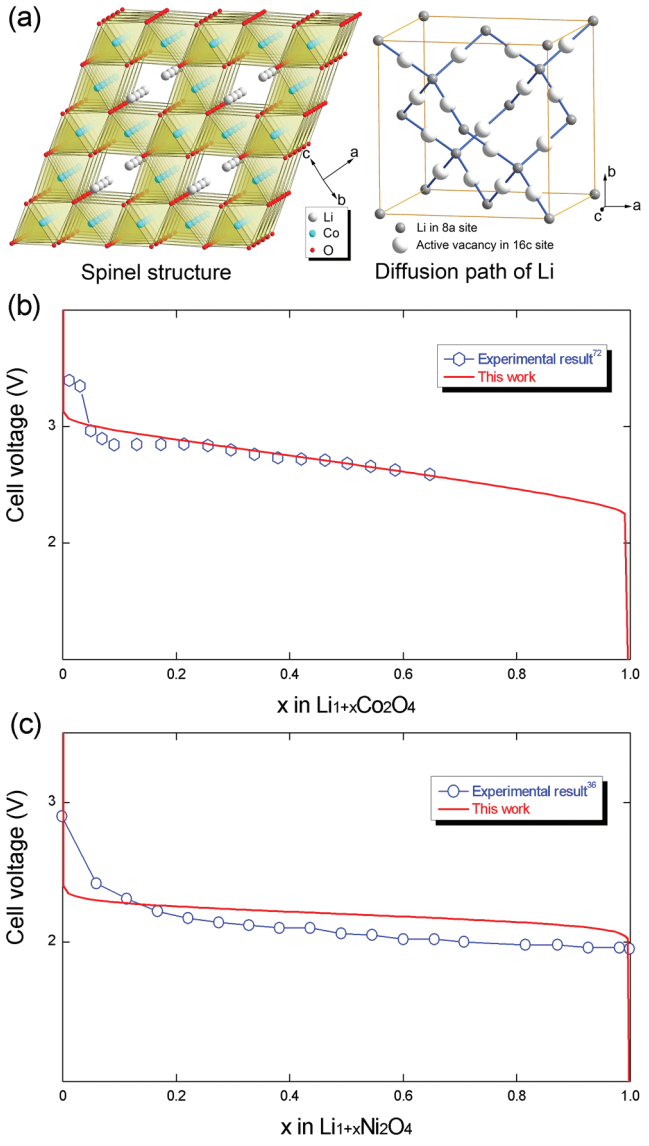

Figure 8. (a) Structure of the spinel phase and the diffusion path of Li in the cathode. (b) Calculated cell voltage of $Li/Li_xCo_2O_4$ ($1 \le x \le 2$) at 300 K compared to the experimental results.[72] (c) Calculated cell voltage of $Li/Li_xNi_2O_4$ ($1 \le x \le 2$) at 300 K compared to the experimental results.[36]

whose structure is also shown in Figure 9a. The cell reaction can be expressed as

$$Li_6CoO_4 \underset{\text{Discharge}}{\overset{\text{Charge}}{\rightleftharpoons}} Li_4CoO_4 + 2Li^+ + 2e$$

The tetragonal/monoclinic phase transformation point has been experimentally determined at $x = 1.0$ by X-ray diffraction.[76] Thus, in our calculation, the interaction parameters for the tetragonal and monoclinic phases are set equal to ensure the correct transformation point. The interaction parameter, −112 397 J/mol, is calculated from the total energies of *t*-Li_4CoO_4, *t*-Li_5CoO_4, and *t*-Li_6CoO_4, using eq 8. Then, the Gibbs energy functions of the tetragonal and monoclinic phases are determined. The calculated cell voltage of $Li/Li_{4+x}CoO_4$ ($0 \le x \le 2$) at 300 K is shown in Figure 9b. Again, the present calculation can reproduce the experimental data reasonably.[76]

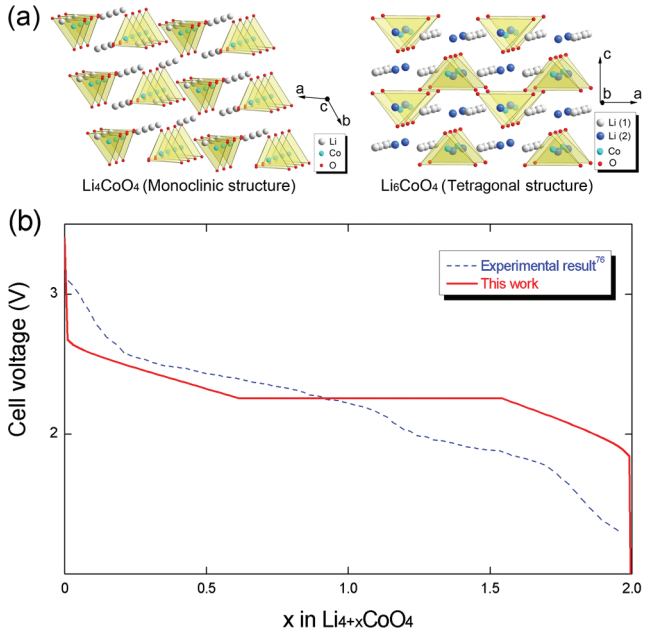

Figure 9. (a) Structure changes in the cathode: monoclinic Li_4CoO_4 and tetragonal Li_6CoO_4. (b) Calculated cell voltage of $Li/Li_{4+x}CoO_2$ ($0 \le x \le 2$) at 300 K, compared to the experimental data.[76]

CONCLUSIONS

In this work, the thermodynamic and electrochemical properties of the Li−Co−O and Li−Ni−O systems have been studied. An approach to accurately calculate enthalpies of formation for transition metal-containing oxides is proposed. The Gibbs energy functions of binary and ternary oxides in the Li−Co−O and Li−Ni−O systems are obtained on the basis of the *ab initio* calculations and empirical predictions. For the oxides of transition metals with valence state +2.7 or +3, the calculated enthalpies of formation at 0 K agree well with available experimental data. However, for oxides of transition metals with valence state of +2 and +4, the data are inconsistent. We propose that the accurate enthalpy of formation per mole metal can be obtained by correcting the pristine GGA data with −0.8 and +0.8 eV shifts for oxides of transition metals with valence state of +2 and +4, respectively. This corrects inaccurately strong correlations of localized and hybridized *d* transition metal states and provides an alternative to the Hubbard approach or the GW approximation. The reliability of the present theoretical approaches is verified by the good agreement between the calculations and experiments for cell voltages of lithium ion batteries.

AUTHOR INFORMATION

Corresponding Author

*E-mail: chang@mch.rwth-aachen.de.

ACKNOWLEDGMENTS

Financial support from the Deutsche Forschungsgemeinschaft (DFG) SPP 1473−WeNDeLIB is gratefully acknowledged.

REFERENCES

(1) Wolverton, C.; Yan, X.-Y.; Vijayaraghavan, R.; Ozolins, V. *Acta Mater.* **2002**, *50*, 2187.

(2) Zhong, Y.; Wolverton, C.; Chang, Y. A.; Liu, Z.-K. *Acta Mater.* **2004**, *52*, 2739.

(3) Zhang, L.; Wang, J.; Du, Y.; Hu, R.; Nash, P.; Lu, X.-G.; Jiang, C. *Acta Mater.* **2009**, *57*, 5324.
(4) Djurovic, D.; Hallstedt, B.; von Appen, J.; Dronskowski, R. *CALPHAD* **2010**, *34*, 279.
(5) Hallstedt, B.; Music, D.; Sun, Z. *Int. J. Mater. Res.* **2006**, *97*, 539.
(6) Wang, L.; Maxisch, T.; Ceder, G. *Phys. Rev. B* **2006**, *73*, 195107.
(7) Chevrier, V.; Ong, S.; Armiento, R.; Chan, M.; Ceder, G. *Phys. Rev. B* **2010**, *82*, 075122.
(8) Van der Ven, A.; Aydinol, M. K.; Ceder, G. *J. Electrochem. Soc.* **1998**, *145*, 2149.
(9) Van der Ven, A.; Ceder, G. *Phys. Rev. B* **1999**, *59*, 742.
(10) Arroyo y de Dompablo, M.; Van der Ven, A.; Ceder, G. *Phys. Rev. B* **2002**, *66*, 064112.
(11) Carlier, D.; Van der Ven, A.; Delmas, C.; Ceder, G. *Chem. Mater.* **2003**, *15*, 2651.
(12) Hwang, B. J.; Tsai, Y. W.; Carlier, D.; Ceder, G. *Chem. Mater.* **2003**, *15*, 3676.
(13) Dudarev, S. L.; Botton, G. A.; Savrasov, S. Y.; Humphreys, C. J.; Sutton, A. P. *Phys. Rev. B* **1998**, *57*, 1505.
(14) Zhou, F.; Cococcioni, M.; Marianetti, C.; Morgan, D.; Ceder, G. *Phys. Rev. B* **2004**, *70*, 235121.
(15) Bréger, J.; Meng, Y. S.; Hinuma, Y.; Kumar, S.; Kang, K.; Shao-Horn, Y.; Ceder, G.; Grey, C. P. *Chem. Mater.* **2006**, *18*, 4768.
(16) Wang, L.; Maxisch, T.; Ceder, G. *Chem. Mater.* **2007**, *19*, 543.
(17) Hinuma, Y.; Meng, Y. S.; Kang, K.; Ceder, G. *Chem. Mater.* **2007**, *19*, 1790.
(18) Kramer, D.; Ceder, G. *Chem. Mater.* **2009**, *21*, 3799.
(19) Kresse, G.; Furthmüller, J. *Phys. Rev. B* **1996**, *54*, 11169.
(20) Kresse, G.; Joubert, D. *Phys. Rev. B* **1999**, *59*, 1758.
(21) Blöchl, P. E. *Phys. Rev. B* **1994**, *50*, 17953.
(22) Monkhorst, H. J.; Pack, J. D. *Phys. Rev. B* **1976**, *13*, 5188.
(23) Farley, T. W. D.; Hayes, W.; Hull, S.; Hutchings, M. T.; Vrtis, M. *J. Phys.: Condens. Matter* **1991**, *3*, 4761.
(24) Cota, L. G.; de la Mora, P. *Acta Crystallogr.* **2005**, *B61*, 133.
(25) Redman, M. J.; Steward, E. G. *Nature* **1962**, *193*, 867.
(26) Yang, M.-C.; Xu, B.; Cheng, J.-H.; Pan, C.-J.; Hwang, B.-J.; Meng, Y. S. *Chem. Mater.* **2011**, *23*, 2832.
(27) Chenavas, J.; Joubert, J. C.; Marezio, M. *Solid State Commun.* **1971**, *9*, 1057.
(28) Smith, W. L.; Hobson, A. D. *Acta Crystallogr.* **1973**, *B29*, 362.
(29) Motohashi, T.; Katsumata, Y.; Ono, T.; Kanno, R.; Karppinen, M.; Yamauchi, H. *Chem. Mater.* **2007**, *19*, 5063.
(30) Arai, H.; Tsuda, M.; Saito, K.; Hayashi, M.; Takei, K.; Sakurai, Y. *J. Solid State Chem.* **2002**, *163*, 340.
(31) Amatucci, G. G.; Tarascon, J. M.; Klein, L. C. *J. Electrochem. Soc.* **1996**, *143*, 1114.
(32) Hirano, A.; Kanno, R.; Kawamoto, Y.; Takeda, Y.; Yamaura, K.; Takano, M.; Ohyama, K.; Ohashi, M.; Yamaguchi, Y. *Solid State Ionics* **1995**, *78*, 123.
(33) Carlier, D.; Saadoune, I.; Croguennec, L.; Ménétrier, M.; Suard, E.; Delmas, C. *Solid State Ionics* **2001**, *144*, 263.
(34) Croguennec, L.; Suard, E.; Willmann, P.; Delmas, C. *Chem. Mater.* **2002**, *14*, 2149.
(35) Antaya, M.; Cearns, K.; Preston, J. S.; Reimers, J. N.; Dahn, J. R. *J. Appl. Phys.* **1994**, *76*, 2799.
(36) Kanno, R.; Kubo, H.; Kawamoto, Y.; Kamiyama, T.; Izumi, F.; Takeda, Y.; Takano, M. *J. Solid State Chem.* **1994**, *110*, 216.
(37) Gummow, R. J.; Liles, D. C.; Thackeray, M. M.; David, W. I. F. *Mater. Res. Bull.* **1993**, *28*, 1177.
(38) Dutta, G.; Manthiram, A.; Goodenough, J. B.; Grenier, J. C. *J. Solid State Chem.* **1992**, *96*, 123.
(39) Jansen, M.; Hoppe, R. *Naturwissenschaften* **1972**, *59*, 215.
(40) Möller, A. *Chem. Mater.* **1998**, *10*, 3196.
(41) Knapp, W. J.; Van Vorst, W. D. *J. Am. Ceram. Soc.* **1951**, *34*, 384.
(42) Huang, G.; Xu, Z. *Thermochim. Acta* **1988**, *136*, 133.
(43) Peng, S.; Grimvall, G. *Int. J. Thermophys.* **1994**, *15*, 973.
(44) Kubaschewski, O.; Alcock, C. B.; Spencer, P. J. *Materials Thermochemistry*, 6th ed.; Pergamon Press: New York, 1993.
(45) Geng, W. T.; Kim, K. S. *Solid State Commun.* **2004**, *129*, 741.
(46) Chen, X.; Huang, D.; Deng, W.; Zhao, Y. *Phys. Lett. A* **2009**, *373*, 391.
(47) Patton, D. C.; Porezag, D. V.; Pederson, M. R. *Phys. Rev. B* **1997**, *55*, 7454.
(48) Hammer, B.; Hansen, L. B.; Nørskov, J. K. *Phys. Rev. B* **1999**, *59*, 7413.
(49) Chase, M. W., Jr. *NIST-JANAF Thermochemical Tables*, 4th ed.; American Institute of Physics: New York, 1998.
(50) Wang, M.; Navrotsky, A. *Solid State Ionics* **2004**, *166*, 167.
(51) Wang, M.; Navrotsky, A.; Venkatraman, S.; Manthiram, A. *J. Electrochem. Soc.* **2005**, *152*, J82.
(52) Wang, M.; Navrotsky, A. *J. Solid State Chem.* **2005**, *178*, 1230.
(53) Loschen, C.; Carrasco, J.; Neyman, K. M.; Illas, F. *Phys. Rev. B* **2007**, *75*, 035115.
(54) Shishkin, M.; Marsman, M.; Kresse, G. *Phys. Rev. Lett.* **2007**, *99*, 246403.
(55) Banus, M. D.; Reed, T. B.; Strauss, A. J. *Phys. Rev. B* **1972**, *5*, 2775.
(56) Reeswinkel, T.; Music, D.; Schneider, J. M. *J. Phys.: Condens. Matter* **2009**, *21*, 145404.
(57) Chang, K.; Hallstedt, B. *CALPHAD* **2011**, *35*, 160.
(58) Chen, M.; Hallstedt, B.; Gauckler, L. *J. Phase Equilib.* **2003**, *24*, 212.
(59) Kowalski, M.; Spencer, P. J. *CALPHAD* **1995**, *19*, 229.
(60) Abe, T.; Koyama, T. *CALPHAD* **2011**, *35*, 209.
(61) Kawaji, H.; Takematsu, M.; Tojo, T.; Atake, T.; Hirano, A.; Kanno, R. *J. Therm. Anal. Calorim.* **2002**, *68*, 833.
(62) Gummow, R. J.; Thackeray, M. M.; David, W. I. F.; Hull, S. *Mater. Res. Bull.* **1992**, *27*, 327.
(63) Croguennec, L.; Pouillerie, C.; Delmas, C. *J. Electrochem. Soc.* **2000**, *147*, 1314.
(64) Arai, H.; Okada, S.; Ohtsuka, H.; Ichimura, M.; Yamaki, J. *Solid State Ionics* **1995**, *80*, 261.
(65) Reimers, J. N.; Dahn, J. R. *J. Electrochem. Soc.* **1992**, *139*, 2091.
(66) Ohzuku, T.; Ueda, A. *J. Electrochem. Soc.* **1994**, *141*, 2972.
(67) Wolverton, C.; Zunger, A. *Phys. Rev. Lett.* **1998**, *81*, 606.
(68) Van der Ven, A.; Aydinol, M. K.; Ceder, G.; Kresse, G.; Hafner, J. *Phys. Rev. B* **1998**, *58*, 2975.
(69) Hong, J.-S.; Selman, J. R. *J. Electrochem. Soc.* **2000**, *147*, 3183.
(70) Arai, H.; Okada, S.; Sakurai, Y.; Yamaki, J.-i. *Solid State Ionics* **1998**, *109*, 295.
(71) Delmas, C.; Ménétrier, M.; Croguennec, L.; Levasseur, S.; Pérès, J. P.; Pouillerie, C.; Prado, G.; Fournès, L.; Weill, F. *Inter. J. Inorg. Mater.* **1999**, *1*, 11.
(72) Meza, E.; Alburquenque, D.; Ortiz, J.; Gautier, J. L. *J. Chil. Chem. Soc.* **2008**, *53*, 1494.
(73) Choi, S.; Manthiram, A. *J. Electrochem. Soc.* **2002**, *149*, A162.
(74) Delmas, C.; Braconnier, J.-J.; Hagenmuller, P. *Mater. Res. Bull.* **1982**, *17*, 117.
(75) Tournadre, F.; Croguennec, L.; Willmann, P.; Delmas, C. *J. Solid State Chem.* **2004**, *177*, 2803.
(76) Narukawa, S.; Takeda, Y.; Nishijima, M.; Imanishi, N.; Yamamoto, O.; Tabuchi, M. *Solid State Ionics* **1999**, *122*, 59.